Electronic Supplementary Material (ESI) for Journal of Materials Chemistry C.

Supplementary Information

Atomic order transition of TiNiPt nanoparticles supported on carbon nanotubes for stable hydrogen evolution reaction

Mengni Wei[a], Mengdi He[a], Xinyu Wei[a], Shen Gong[a,b,c,*], Liuxiong Luo[a], Teng Li[a], Shanguang Tang[d] and Zhenghong Zhu[c]

a. School of Materials Science and Engineering, Central South University, Hunan, Changsha 410083, China.
b. State Key Laboratory of Powder Metallurgy, Changsha 410083, China.
c. Department of Mechanical Engineering, York University, 4700 Keele Street, Toronto, ON, M3J 1P3, Canada.
d. Hunan Yige Pharmaceutical Co.,Ltd， Xiangtan 411100，China.
**Corresponding author: Shen Gong (gongshen011@csu.edu.cn).*

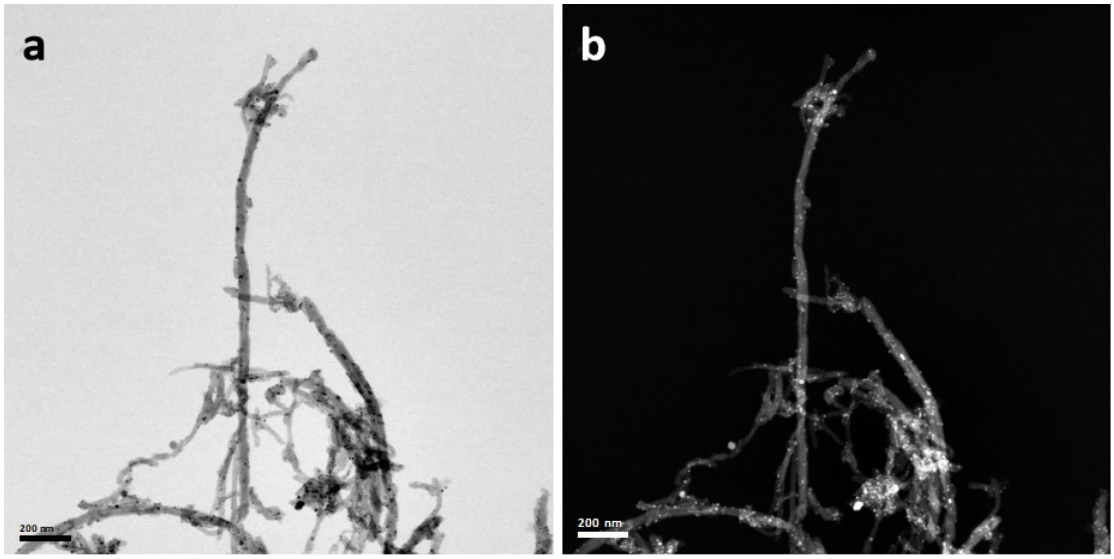

Fig. S1 (a)TEM bright field image and (b) dark field image of disordered $Ti_{50}Ni_{30}Pt_{20}$/CNT

The TEM photos of disordered $Ti_{50}Ni_{30}Pt_{20}$/CNT are shown in Fig. S1. Disordered TiNiPt alloy nanoparticles are dispersed and evenly wrapped on the surface of carbon nanotubes. Its particle size is 8-10 nm.

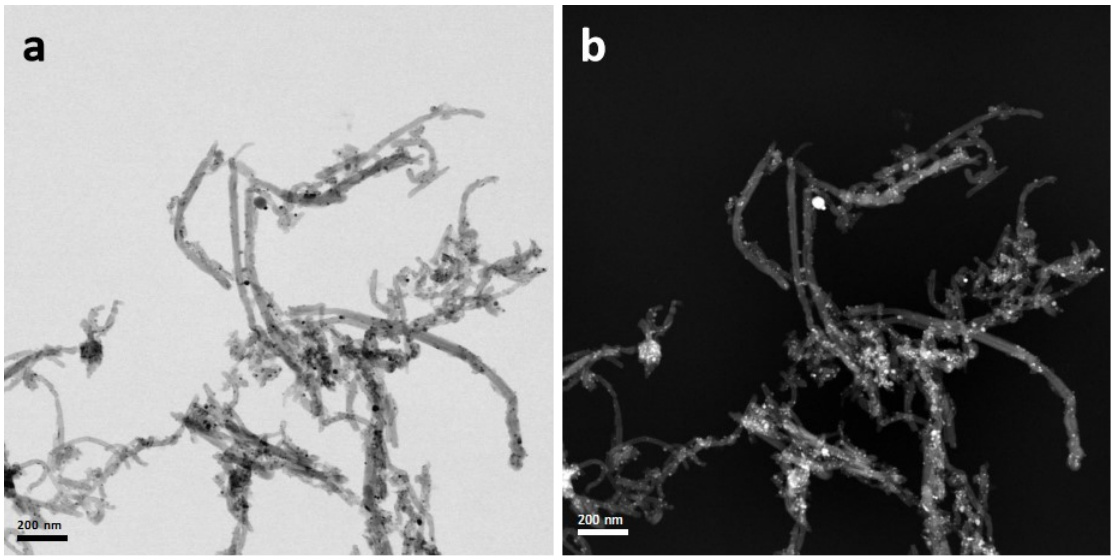

Fig. S2 (a)TEM bright field image and (b) dark field image of ordered $Ti_{50}Ni_{30}Pt_{20}$/CNT

Fig. S2 shows the morphological features of the ordered $Ti_{50}Ni_{30}Pt_{20}$/CNT by TEM. The ordered TiNiPt alloy nanoparticles are uniformly supported on the surface of carbon nanotubes. Its particle size is about 9-11 nm, which is similar to that of disordered TiNiPt alloy nanoparticles. It is an effective strategy to select carbon nanotubes as carriers for interfacial confinement of alloy particles.

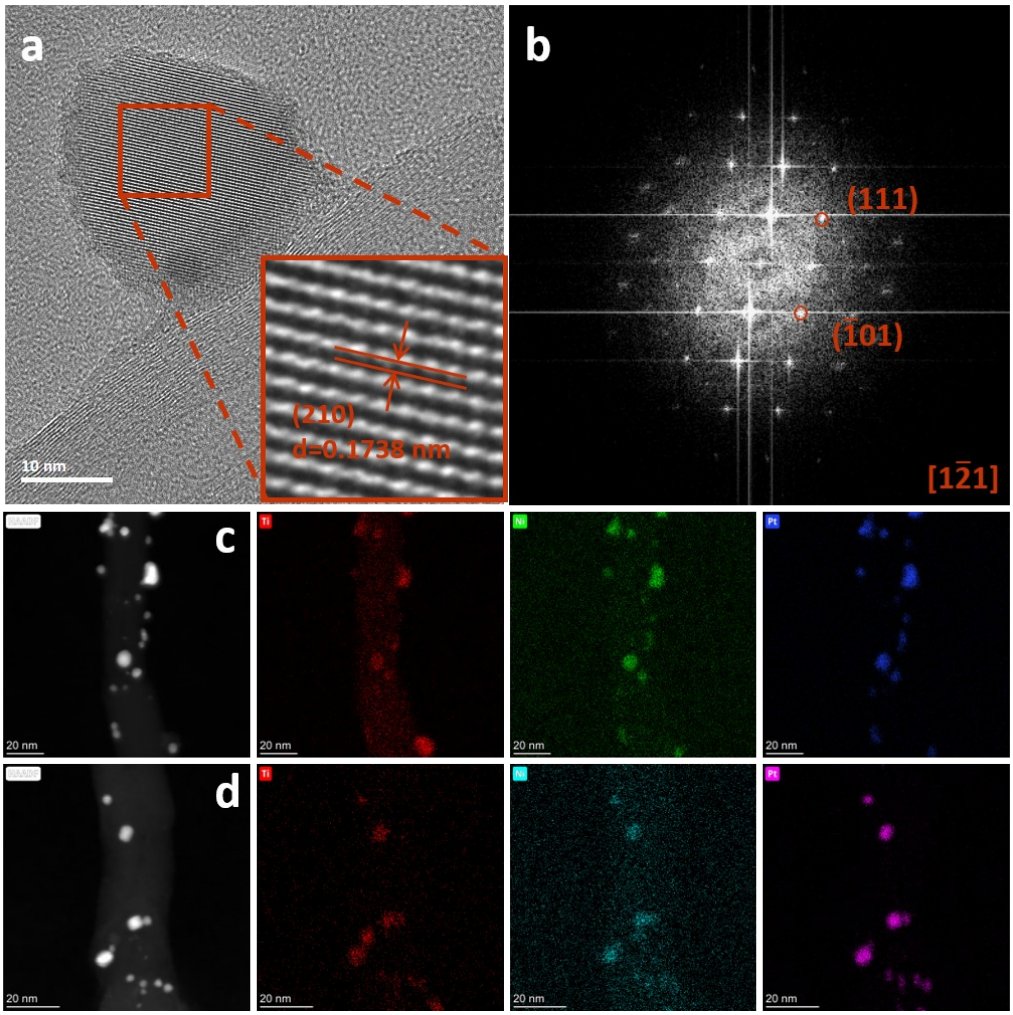

Fig. S3 (a) TEM high-resolution images of O-$Ti_{50}Ni_{30}Pt_{20}$/CNT. (b) FFT patterns of (a). (c,d) HADDF and EDS element mappings of O-$Ti_{50}Ni_{30}Pt_{20}$/CNT.

In Fig. S3a, lattice fringes with spacing of 0.1738 nm correspond to (210) crystal planes. In the FFT image of Fig. S4b, the appearance of superlattice diffraction points ($10\bar{1}$), (111), etc. indicates the formation of ordered TiNiPt particles. In EDS element mappings (Fig. S3c and d), Ti, Ni and Pt elements always appear in the same region, indicating that the particles are mainly ternary phases of TiNiPt.

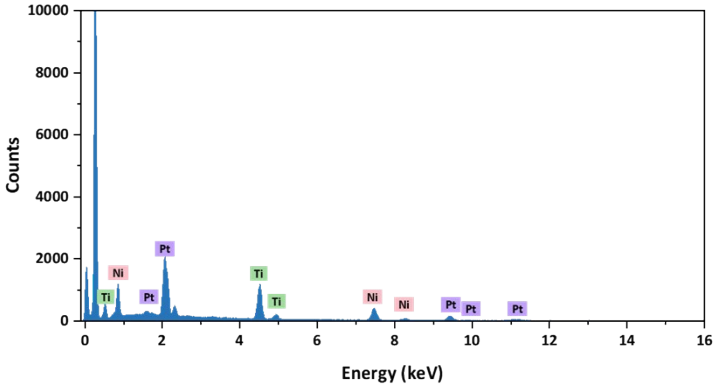

Element	Atomic %
Ti	45.85
Ni	31.17
Pt	22.99

Fig. S4 SEM EDS spectra and atomic ratio of a selected individual $Ti_{50}Ni_{30}Pt_{20}$ particle

Representative SEM EDS spectra of $Ti_{50}Ni_{30}Pt_{20}$/CNT are shown in Fig. S4. The atomic ratio of Ti, Ni to Pt in this sample is 0.459:0.312:0.230, which is very close to the formulation addition of 0.5:0.3:0.2.

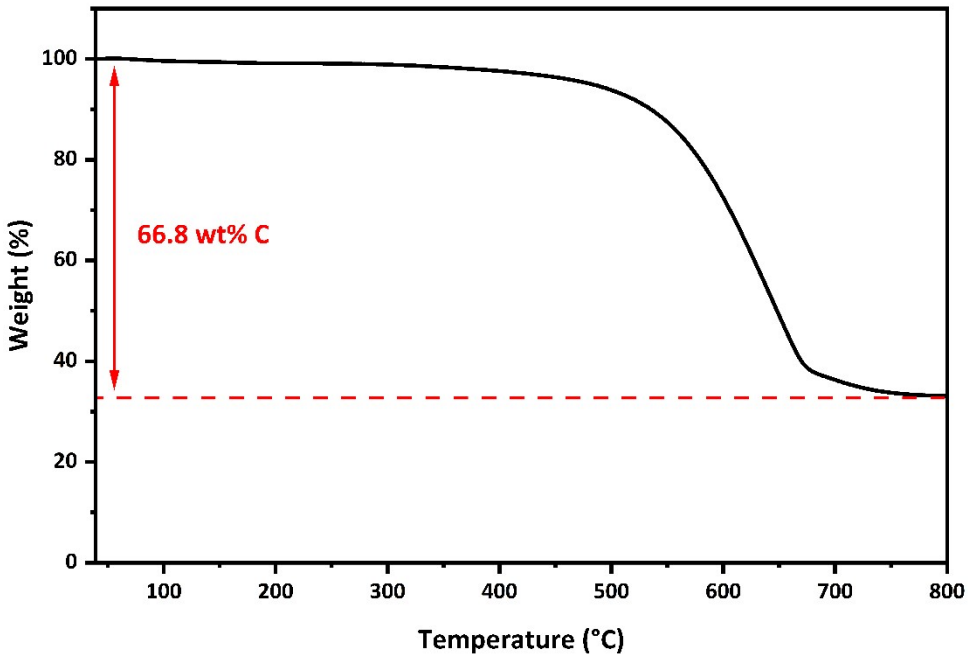

Fig. S5 TGA curve of O-$Ti_{50}Ni_{30}Pt_{20}$/CNT

The TGA experiments are performed on O-$Ti_{50}Ni_{30}Pt_{20}$/CNT to determine the metal loadings. The temperature is raised from room temperature to 800°C at a heating rate of 10°C/min. The protective atmosphere is air. The loss of 66.8 wt.% is attributed to the burning of CNTs in air. Therefore, the metal loading is about 33.2 wt.%.

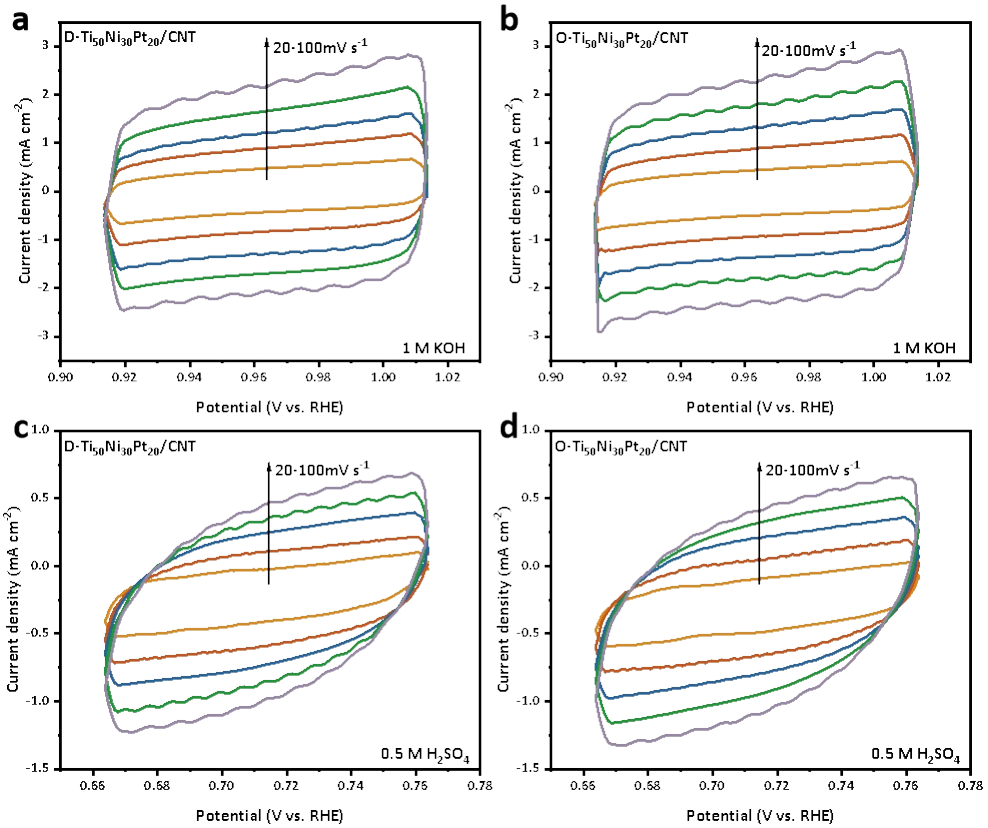

Fig. S6 (a, b) Electrochemical cyclic voltammetry of D-$Ti_{50}Ni_{30}Pt_{20}$/CNT and O-$Ti_{50}Ni_{30}Pt_{20}$/CNT in 1 M KOH. (c, d) Electrochemical cyclic voltammetry of D-$Ti_{50}Ni_{30}Pt_{20}$/CNT and O-$Ti_{50}Ni_{30}Pt_{20}$/CNT in 0.5 M H_2SO_4. The scan rates are 20, 40, 60, 80 and 100 mV s^{-1}.

To further understand the HER performance of D-$Ti_{50}Ni_{30}Pt_{20}$/CNT and O-$Ti_{50}Ni_{30}Pt_{20}$/CNT, their electrochemically active surface area (ECSA) was estimated from the electrochemical double layer capacitance (Cdl). Cdl was measured from a cyclic voltammogram (CV) in the Faraday region. The calculated Cdl of D-$Ti_{50}Ni_{30}Pt_{20}$/CNT and O-$Ti_{50}Ni_{30}Pt_{20}$/CNT are 22.32 and 20.67 mF cm^{-2} in 1 M KOH. And their calculated Cdl are 6.92 and 6.53 mF cm^{-2} in 0.5 M H_2SO_4.

Table S1. Summarized HER performance of commercial Pt/C, disordered and ordered TiNiPt/CNT samples in 1 M KOH.

Samples	Overpotential at 10 mA cm^{-2} (mV)	Tafel slope (mV dec^{-1})	Exchange current density (mA cm^{-2})
20% Pt/C	41	43.7	0.84
D-$Ti_{50}Ni_{40}Pt_{10}$/CNT	43	47.3	1.24
D-$Ti_{50}Ni_{30}Pt_{20}$/CNT	25	30.9	1.45
D-$Ti_{50}Ni_{20}Pt_{30}$/CNT	35	34.8	0.95
D-$Ti_{50}Ni_{10}Pt_{40}$/CNT	38	43.1	1.43
O-$Ti_{50}Ni_{40}Pt_{10}$/CNT	25	32.4	1.65
O-$Ti_{50}Ni_{30}Pt_{20}$/CNT	21	25.7	1.46
O-$Ti_{50}Ni_{20}Pt_{30}$/CNT	30	37.5	1.25
O-$Ti_{50}Ni_{10}Pt_{40}$/CNT	40	31.3	1.58

Table S2. Summarized HER performance of commercial Pt/C, disordered and ordered TiNiPt/CNT samples in 0.5 M H_2SO_4.

Samples	Overpotential at 10 mA cm^{-2} (mV)	Tafel slope (mV dec^{-1})	Exchange current density (mA cm^{-2})
20% Pt/C	40	38.4	0.531
D-$Ti_{50}Ni_{40}Pt_{10}$/CNT	49	45.5	0.772
D-$Ti_{50}Ni_{30}Pt_{20}$/CNT	39	31.6	0.613
D-$Ti_{50}Ni_{20}Pt_{30}$/CNT	48	38.4	0.721
D-$Ti_{50}Ni_{10}Pt_{40}$/CNT	44	44.6	0.509
O-$Ti_{50}Ni_{40}Pt_{10}$/CNT	52	43.8	0.581
O-$Ti_{50}Ni_{30}Pt_{20}$/CNT	36	28.7	0.565
O-$Ti_{50}Ni_{20}Pt_{30}$/CNT	43	37.4	0.553
O-$Ti_{50}Ni_{10}Pt_{40}$/CNT	47	43.1	0.502

Table S3. Comparison of HER performance of recently reported catalysts.

Catalyst	Overpotential at 10 mA cm^{-2} (mV)	Tafel slope (mV dec^{-1})	Exchange current density (mA cm^{-2})	Electrolyte	Ref.
20% Pt/C	41	43.7	0.84	1 M KOH	This work
O-$Ti_{50}Ni_{30}Pt_{20}$/CNT	21	25.7	1.46	1 M KOH	This work
Pt-PdO/C	29	36	1.125	1 M KOH	1
PtSA–$Co(OH)_2$@Ag NW	29	35.72	0.82	1 M KOH	2
Rh NSs	37.8	98.3	3.68	1 M KOH	3
Ru@MWCNT	17	27	2.4	1 M KOH	4
RuP_2@NPC/CNT	12	30	4.0	1 M KOH	5
Ru-Mo_2C@CNT	15	26	4.3	1 M KOH	6
IrPdPb WNNs	21	66	4.87	1 M KOH	7
PtCu-MoO_2@C	24	37	2.25	1 M KOH	8
$(Ni,Co)_3$CNSs@NC	71	72	0.61	1 M KOH	9
2D-PtND/LDH	25	87	1.65	1 M KOH	10
CoP@N,S-3D-GN	118	50	0.022	0.5 M H_2SO_4	11
Pt-TiO_2-x NSs	36	32.1	1.04 ± 0.3	0.5 M H_2SO_4	12
PtW NPs/C	19.4	27.8	1.62	0.5 M H_2SO_4	13
N-Co-S/G	67.7	56.3	0.901	0.5 M H_2SO_4	14
Mo_2C/CNT	121	77	2.02	0.5 M H_2SO_4	15
MRNS	29.4	30.9	1.12	0.5 M H_2SO_4	16
Pt-MoS_2-1h	78.5	41	0.3375	0.5 M H_2SO_4	17
Pt-MoS_2/MWCNT fiber	40	30	0.4554	0.5 M H_2SO_4	18
WC/WO_{3-x}-900	107	59.3	0.253	0.5 M H_2SO_4	19
Co-MoS_2/G	78.1	40.0	0.0917	0.5 M H_2SO_4	20
C/Ni–AuPt	131	66	0.125	0.5 M H_2SO_4	21
20% Pt/C	40	38.4	0.531	0.5 M H_2SO_4	This work
O-$Ti_{50}Ni_{30}Pt_{20}$/CNT	36	28.7	0.565	0.5 M H_2SO_4	This work

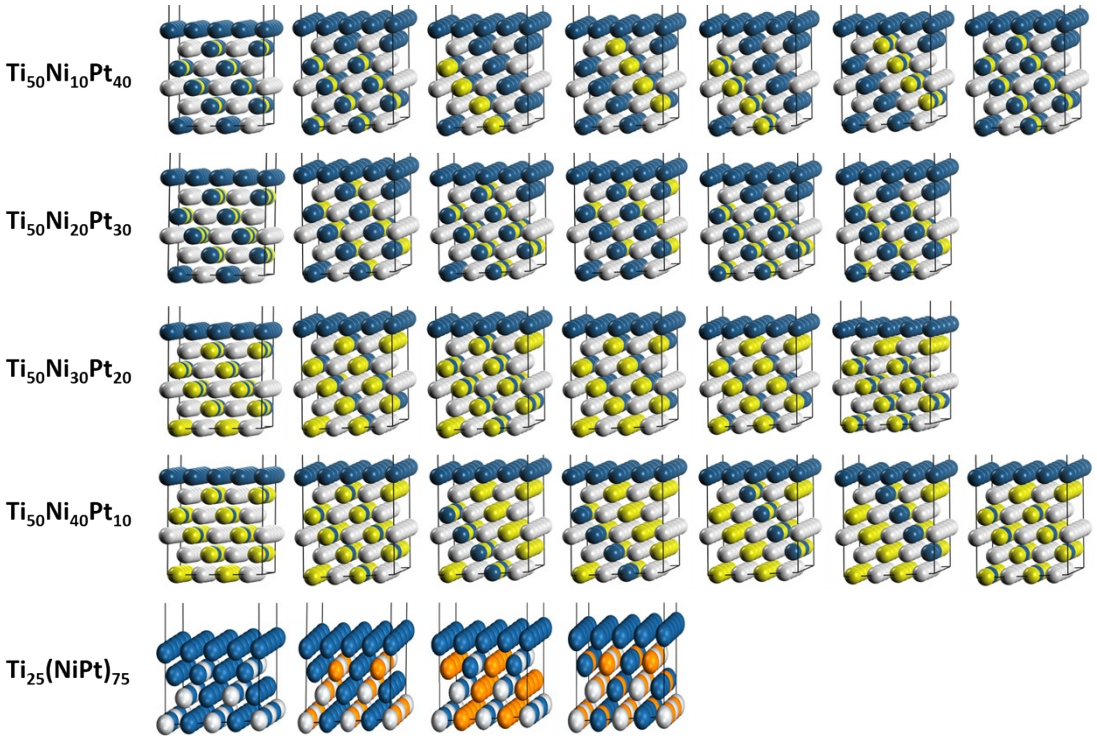

Fig. S7 DFT atomic models for different atomic ratios and positions

First-principles calculations are used to assist in the study of the effects of atomic positions and ratios on the performance of samples. A series of atomic models have been established, including different atomic ratios and positions. The model energy is lowest when the atom is in a highly symmetrical position. The calculation results of this model are placed in the main text.

Table S4. Comparison of free energies ΔG_{HO-H} and ΔG_{H^*} in HER of catalysts.

	ΔG_{HO-H} (eV)	ΔG_{H^*} (eV)	Ref.
O-$Ti_{50}Ni_{30}Pt_{20}$/CNT	0.28	-0.37	This work
NiO/Pt	0.58	-0.06	22
$Pt_{22}Ru_{33}$/BP	-	-0.12	23
Pt/$Co_{0.85}Se$	0.443	Co site -0.083 Pt site -0.079	24
Pt/NiFe-LDH	-0.41	-0.15	25
$Ni_2P/Ni(PO_3)_2$	-0.33	-0.05	26
TFPB-PAM	-	0.0705	27
Pt SACs	-	Pt/basal graphene 0.57 Pt/edge graphene -0.26	28
Pt_{SA}-Ni	0.08	-0.38	29

References

1. R. Samanta, R. Mishra and S. Barman, *ACS Sustainable Chemistry & Engineering*, 2022, **10**, 3704-3715.
2. K. L. Zhou, C. Wang, Z. Wang, C. B. Han, Q. Zhang, X. Ke, J. Liu and H. Wang, *Energy & Environmental Science*, 2020, **13**, 3082-3092.
3. Z. Zhang, G. Liu, X. Cui, Y. Gong, D. Yi, Q. Zhang, C. Zhu, F. Saleem, B. Chen, Z. Lai, Q. Yun, H. Cheng, Z. Huang, Y. Peng, Z. Fan, B. Li, W. Dai, W. Chen, Y. Du, L. Ma, C.-J. Sun, I. Hwang, S. Chen, L. Song, F. Ding, L. Gu, Y. Zhu and H. Zhang, *Science Advances*, **7**, eabd6647.
4. D. H. Kweon, M. S. Okyay, S.-J. Kim, J.-P. Jeon, H.-J. Noh, N. Park, J. Mahmood and J.-B. Baek, *Nature Communications*, 2020, **11**, 1278.
5. F. Zhou, R. Sa, X. Zhang, S. Zhang, Z. Wen and R. Wang, *Applied Catalysis B: Environmental*, 2020, **274**, 119092.
6. X. Wu, Z. Wang, D. Zhang, Y. Qin, M. Wang, Y. Han, T. Zhan, B. Yang, S. Li, J. Lai and L. Wang, *Nature Communications*, 2021, **12**, 4018.
7. R.-L. Zhang, J.-J. Duan, L.-P. Mei, J.-J. Feng, P.-X. Yuan and A.-J. Wang, *Journal of Colloid and Interface Science*, 2020, **580**, 99-107.
8. C. Zhang, P. Wang, W. Li, Z. Zhang, J. Zhu, Z. Pu, Y. Zhao and S. Mu, *Journal of Materials Chemistry A*, 2020, **8**, 19348-19356.
9. M. Yao, B. Wang, N. Wang, S. Komarneni, Y. Chen, J. Wang, X. Niu and W. Hu, *ACS Sustainable Chemistry & Engineering*, 2020, **8**, 5287-5295.
10. Y.-R. Hong, S. Dutta, S. W. Jang, O. F. Ngome Okello, H. Im, S.-Y. Choi, J. W. Han and I. S. Lee, *Journal of the American Chemical Society*, 2022, **144**, 9033-9043.
11. C. Karaman, O. Karaman, N. Atar and M. L. Yola, *Electrochimica Acta*, 2021, **380**, 138262.
12. K. M. Naik, E. Higuchi and H. Inoue, *Nanoscale*, 2020, **12**, 11055-11062.
13. D. Kobayashi, H. Kobayashi, D. Wu, S. Okazoe, K. Kusada, T. Yamamoto, T. Toriyama, S. Matsumura, S. Kawaguchi, Y. Kubota, S. M. Aspera, H. Nakanishi, S. Arai and H. Kitagawa, *Journal of the American Chemical Society*, 2020, **142**, 17250-17254.
14. P. Sabhapathy, I. Shown, A. Sabbah, P. Raghunath, J.-L. Chen, W.-F. Chen, M.-C. Lin, K.-H. Chen and L.-C. Chen, *Nano Energy*, 2021, **80**, 105544.
15. S. Hussain, I. Rabani, D. Vikraman, A. Feroze, K. Karuppasamy, Z. u. Haq, Y.-S. Seo, S.-H. Chun, H.-S. Kim and J. Jung, *ACS Sustainable Chemistry & Engineering*, 2020, **8**, 12248-12259.
16. J. Kim, K. Kani, J. Kim, J. S. Yeon, M.-K. Song, B. Jiang, J. Na, Y. Yamauchi and H. S. Park, *Journal of Industrial and Engineering Chemistry*, 2021, **96**, 371-375.
17. L. Mei, X. Gao, Z. Gao, Q. Zhang, X. Yu, A. L. Rogach and Z. Zeng, *Chemical Communications*, 2021, **57**, 2879-2882.
18. B. Chen, G. Sun, J. Wang, G. Liu, C. Tan, Y. Chen, H. Cheng, J. Chen, Q. Ma, L. Huang, P. Chen and H. Zhang, *Chemical Communications*, 2020, **56**, 5131-5134.
19. F. Wang, B. Dong, J. Wang, N. Ke, C. Tan, A. Huang, Y. Wu, L. Hao, L. Yin, X. Xu, Y. Xian and S. Agathopoulos, *Journal of Advanced Ceramics*, 2022, **11**, 1208-1221.
20. S. Sarwar, M.-C. Lin, M. R. Ahasan, Y. Wang, R. Wang and X. Zhang, *Advanced Composites and Hybrid Materials*, 2022, DOI: 10.1007/s42114-022-00424-3.
21. Y. Yu, S. J. Lee, J. Theerthagiri, S. Fonseca, L. M. C. Pinto, G. Maia and M. Y. Choi, *Chemical*

Engineering Journal, 2022, **435**, 134790.

22. Z.-J. Chen, G.-X. Cao, L.-Y. Gan, H. Dai, N. Xu, M.-J. Zang, H.-B. Dai, H. Wu and P. Wang, *ACS Catalysis*, 2018, **8**, 8866-8872.
23. Y. Li, W. Pei, J. He, K. Liu, W. Qi, X. Gao, S. Zhou, H. Xie, K. Yin, Y. Gao, J. He, J. Zhao, J. Hu, T.-S. Chan, Z. Li, G. Zhang and M. Liu, *ACS Catalysis*, 2019, **9**, 10870-10875.
24. K. Jiang, B. Liu, M. Luo, S. Ning, M. Peng, Y. Zhao, Y.-R. Lu, T.-S. Chan, F. M. F. de Groot and Y. Tan, *Nature Communications*, 2019, **10**, 1743.
25. Y. Zhao, Y. Gao, Z. Chen, Z. Li, T. Ma, Z. Wu and L. Wang, *Applied Catalysis B: Environmental*, 2021, **297**, 120395.
26. Z. Xiao, M. Yang, C. Liu, B. Wang, S. Zhang, J. Liu, Z. Xu, R. Gao, J.-J. Zou, A. Tang and H. Yang, *Nano Energy*, 2022, **98**, 107233.
27. A. Pradhan and R. N. Manna, *ACS Applied Polymer Materials*, 2021, **3**, 1376-1384.
28. C. Tsounis, B. Subhash, P. V. Kumar, N. M. Bedford, Y. Zhao, J. Shenoy, Z. Ma, D. Zhang, C. Y. Toe, S. Cheong, R. D. Tilley, X. Lu, L. Dai, Z. Han and R. Amal, *Advanced Functional Materials*, 2022, **n/a**, 2203067.
29. K. L. Zhou, Z. Wang, C. B. Han, X. Ke, C. Wang, Y. Jin, Q. Zhang, J. Liu, H. Wang and H. Yan, *Nature Communications*, 2021, **12**, 3783.